NEURIT: Pushing the Limit of Neural Inertial Tracking for Indoor Robotic IoT

Xinzhe Zheng[†], Sijie Ji[‡], Yipeng Pan[†], Kaiwen Zhang[§], Chenshu Wu[‡]

Department of Computer Science, The University of Hong Kong

[†]{zxz.krypton, pan.yp}@outlook.com [‡]{sijieji, chenshu}@cs.hku.hk [§]zhangkev@connect.hku.hk

Abstract—Inertial tracking is vital for robotic IoT and has gained popularity thanks to the ubiquity of low-cost Inertial Measurement Units (IMUs) and deep learning-powered tracking algorithms. Existing works, however, have not fully utilized IMU measurements, particularly magnetometers, nor maximized the potential of deep learning to achieve the desired accuracy. To enhance the tracking accuracy for indoor robotic applications, we introduce NEURIT, a sequence-to-sequence framework that elevates tracking accuracy to a new level. NEURIT employs a Time-Frequency Block-recurrent Transformer (TF-BRT) at its core, combining the power of recurrent neural network (RNN) and Transformer to learn representative features in both time and frequency domains. To fully utilize IMU information, we strategically employ body-frame differentiation of the magnetometer, which considerably reduces the tracking error. NEURIT is implemented on a customized robotic platform and evaluated in various indoor environments. Experimental results demonstrate that NEURIT achieves a mere 1-meter tracking error over a 300-meter distance. Notably, it significantly outperforms state-of-the-art baselines by 48.21% on unseen data. NEURIT also performs comparably to the visual-inertial approach (Tango Phone) in vision-favored conditions and surpasses it in plain environments. We believe NEURIT takes an important step forward toward practical neural inertial tracking for ubiquitous and scalable tracking of robotic things. NEURIT, including the source code and the dataset, is open-sourced here: https://github.com/NeurIT-Project/NeurIT.

Index Terms—neural inertial tracking, indoor robotic localization, inertial measurement unit, time-frequency learning.

Figure 1: Tracking performance comparison and visualization of estimated trajectories.

I. INTRODUCTION

Indoor tracking is vital for robots, as it allows them to provide location-based services and navigate in areas where satellite signals are weak or unavailable. Numerous techniques have been investigated for this purpose. Vision-based methods [1] show remarkable performance in favorable environments, yet degrade in plain environments and bad lighting conditions.

LiDAR has been used to generate accurate tracking and mapping [2], which, however, is too costly and may suffer from severe drift in the absence of environmental feature points. Wireless tracking solutions utilizing WiFi [3], millimeter-wave [4], or ultra-wide bandwidth (UWB) [5] technologies have also been widely studied, yet the performance is not robust in real-world cases while the deployment overhead is significant. These methodologies either rely on external infrastructure or depend on environmental features. In contrast, inertial tracking using IMUs has carved a niche by offering a truly infrastructure-free solution [6]. An IMU is a self-contained module 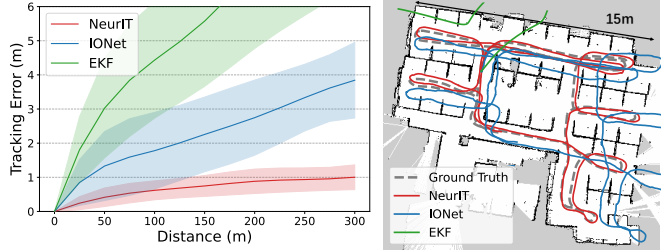integrating accelerometer, gyroscope, and magnetometer, which is a standard component in ubiquitous devices including commercial robots. IMU-based tracking method does not depend on external infrastructure, rendering an inside-out solution that is suitable for indoor robotic navigation in various conditions.

However, achieving high accuracy in inertial tracking is challenging due to sensor noise and drifts. Conventional studies examine filtering techniques like Kalman filter [7], complementary filter [8], etc., to reduce IMU noise. These techniques may not work well in distinct conditions or for long duration. The emergence of machine learning, specifically neural inertial tracking based on deep neural networks, offers a new approach that promises improved precision and generalizability.

Two types of neural networks are mainly exploited: RNN and Transformers. Despite acceptable results, they face limitations, particularly on cross-domain or unseen datasets, leaving considerable scope for refinement to realize the full potential of deep learning in inertial tracking.

- RNN-based solutions can capture temporal features well [9]–[12]. However, their operational inefficiency and the short-term memory causing vanishing gradients [13] can destabilize learning outcomes.
- Transformers for inertial tracking [14], [15] have shown promising results. However, they struggle to capture information beyond the perception field, especially essential past data for the current motion context. Additionally, performance drops on unseen datasets indicate insufficient generalization capabilities based on their reports.
- Existing works mostly employ accelerations and gyroscopes only and exclude the magnetometer for learning. Few works have integrated magnetometers for drift compensation, yet merely employ complementary filter-based techniques [12], [16], yielding only marginal enhancements in the outcomes.

To overcome these limitations, we present NEURIT, a novel system that unleashes the full potential of neural inertial tracking and achieves remarkable accuracy for robotic tracking. NEURIT excels mainly in two aspects: First, based on an in-depth understanding of inertial data properties, NEURIT incorporates magnetometer data as an additional feature with accelerometer and gyroscope measurements. While it has been believed that the magnetometer is susceptible to indoor interference [17]–[19] and is excluded from learning previously, we notice that it has a lower drift than the gyroscope in providing long-term orientation information, rendering it a valuable input for potential drift compensation. It is noticeable that magnetometers primarily capture pose information, while accelerations and gyroscopes depict the movement at a fine-grained level. To align these features together, we integrate *magnetometer differentiation within the body frame*. This ensemble enhances the network's ability to counteract the noise-induced drift in pose estimation. Second, to maximize the potential of neural networks for enhanced inertial tracking, we propose a novel *Time-frequency Block-Recurrent Transformer*, named TF-BRT, which embraces the advantages of both RNN and Transformer and overcomes their respective drawbacks by extracting pre-sequence information and local motion information within the perception field. Particularly, TF-BRT extracts both time and frequency domain information to obtain a more comprehensive understanding of object movement. By learning from complete IMU data with an advanced neural network design, NEURIT achieves robust tracking capabilities that endure extended duration and cover substantial distances.

To implement and evaluate NEURIT, we build a customized robotic platform, which consists of a commodity 9-axis IMU for NEURIT, a LiDAR-inertial system for ground truth, and a visual-inertial system for comparison. We verify the performance of NEURIT on two public benchmarks and a newly built dataset. Our own dataset is collected in three different campus buildings, totaling 33.7 km over about 15 hours. The experimental results demonstrate that NEURIT not only outperforms all baseline models in the existing benchmark dataset, it also achieves better results under more challenging, practical conditions. Specifically, compared with the best baseline, NEURIT improves the tracking accuracy by 48.21% on unseen data and achieves an average drift rate of 0.62%, indicating its superior robustness over long distances. Additionally, NEURIT achieves the thus far best performance on two benchmark datasets, RIDI [20] and RONIN [9]. Further, when compared to commercial visual-inertial algorithm [21], NEURIT exceeds in plain environments while achieving comparable performance in visual-favored environments. Fig. 1 illustrates the superior tracking accuracy achieved by NEURIT, while previous neural inertial tracking algorithm (IONet [10]) and traditional control algorithm (EKF [7]) fail to provide robust tracking outcomes. This enhances the potential of inertial tracking as a viable solution for various indoor tracking applications and invites new perspectives on the longstanding challenge of indoor positioning.

In summary, our core contributions are as follows:

1) With in-depth insight into IMU, we integrate magnetometers for neural inertial tracking. We propose an effective sensor fusion approach by using the derivative of body-frame magnetometers, which demonstrates substantial enhancements in tracking accuracy and robustness.
2) We propose NEURIT, an inertial tracking system that leverages a full set of IMU data under a novel network design named TF-BRT. TF-BRT exploits the advantages of both RNN and Transformer and effectively learns from time-frequency domain information, enabling accurate tracking in various environments and minimizing drift over extended periods and distances.
3) We implement NEURIT with a customized robotic platform and test it in various environments using a newly built dataset. NEURIT surpasses the existing baselines on all the benchmark datasets and performs well against a visual-inertial tracking system. We have open-sourced the collected dataset and source code for the research community.

In the rest of the paper, we investigate the insights of neural inertial tracking in §II and present the system design in §III. We present implementation details in §IV, followed by experiment settings in §V. We evaluate NEURIT scrupulously in §VI. Finally, we review the literature in §VII and conclude the paper in §VIII.

II. OBSERVATIONS AND MEASUREMENTS

IMU-based tracking often suffers from orientation drift, which is mainly caused by gyroscope noises. In outdoor scenarios, global magnetometers can correct the drift to some extent. Nevertheless, in indoor environments, ferromagnetic materials in building structures can distort magnetometers [17], [18]. This potential distortion serves as a potential consideration, possibly explaining the omission of magnetometers as input features in prior neural inertial tracking studies. To test this hypothesis, we collected magnetometer and gyroscope data from different indoor environments and used them to estimate the heading orientations. We then compared the accuracy of each method by calculating the heading error over time and plotting the results in Fig. 2. The first row represents the heading error outcomes given by global magnetometers and gyroscopes. From the dashed lines, despite the impact of complex buildings on global magnetometers and the presence of fluctuating orientation errors, the long-term orientation drift of global magnetometers is minimal compared to gyroscope-derived heading directions. This intriguing finding leads us to posit that magnetometers could serve as a viable compensatory feature in the context of neural inertial tracking.

Nevertheless, how to encapsulate the three modalities remains a challenge, given their unique perspectives on measuring the target's motion. First, for precise floor plane tracking, converting accelerations and gyroscopes from the IMU body frame to the Earth frame is crucial since the IMU operates in a non-inertial coordinate system. Unlike accelerometers and gyroscopes, which measure the amount of motion but not the precise direction, magnetometers can directly infer the orientation of an object. To improve the alignment of
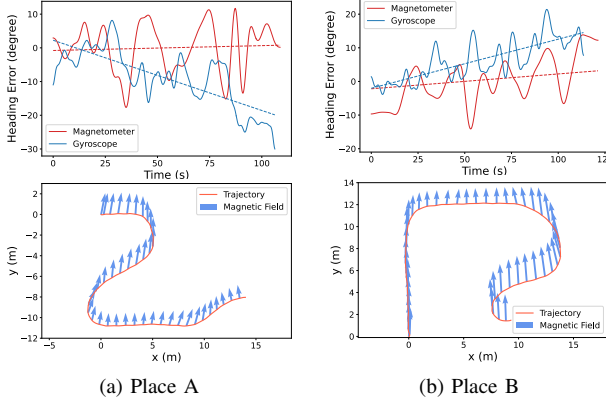
(a) Place A (b) Place B

Figure 2: Global magnetometers study in the indoor environment. The first row shows the heading error comparison between global magnetometers and gyroscopes, which indicates that magnetometers can be used for orientation drift compensation from gyroscopes. The second row illustrates the orientation of global magnetometers on the floor plane.

magnetometers with accelerometers and gyroscopes, we introduce the *derivative of magnetometers in the body frame*, which encompasses both the pose information and the object's orientation motion, enhancing the network's ability to learn motion patterns at a finer-grained level. We believe it can be a powerful compensation feature for indoor tracking tasks, culminating in the sensor-fusion algorithm for our neural inertial tracking method. In section §VI-E, we conduct a study with magnetometers, which shows the superior performance of incorporating magnetometer data into our system.

III. NEURIT DESIGN

A. Overview

NEURIT presents a sequence-to-sequence framework to reconstruct the moving trajectories of robots using low-cost IMU sensors only, without relying on any external infrastructure (*e.g.*, Access Points, cellular stations). Fig. 3 overviews the design of NEURIT. To track the robot's movement, IMU readings that consist of accelerations, gyroscopes, and magnetometers are collected and pre-processed into a time series representation. The core of NEURIT is a neural network called TF-BRT, a novel model that leverages block-recurrent attention [22] and time-frequency learning. The block-recurrent attention mechanism allows the neural network to incorporate both the current IMU data and the historical information to produce a more accurate tracking result. Moreover, the input includes both time and frequency domain features, enhancing its inference ability for different motion states. At the end of NEURIT, the output generated by TF-BRT, which is a sequence of movement speed and orientation, is integrated to calculate the robot's location at any time. We consider predicting the robot's location directly is not an effective option because locations do not constitute a finite set. Additionally, we introduce a multi-
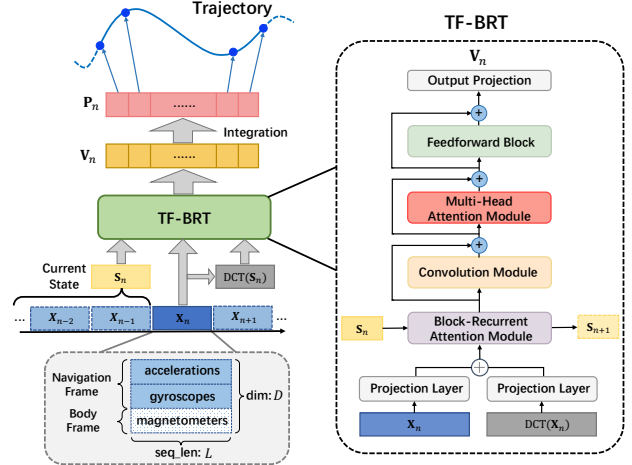

Figure 3: NEURIT Overview. Left side: End-to-end indoor tracking framework; Right side: TF-BRT architecture.

loss learning method and data augmentation to further enhance the robustness of TF-BRT.

B. Data Preparation

IMU coordinate frame, which changes all the time, reports the raw IMU data. The Earth coordinate frame, on the other hand, defines the moving trajectory. To resolve this discrepancy, coordinate transformation is required. A common practice in neural inertial tracking [9] is to transform both the raw IMU data and the ground truth into the same coordinate frame, which is called the navigation frame. We use the same coordinate frame transformation as RONIN [9] in NEURIT, which uses a *heading-agnostic coordinate frame* (Earth coordinate frame) to represent the IMU data.

The coordinate transformation is only applied to accelerations and gyroscopes:

$$(\mathbf{a}^g, \mathbf{w}^g) = \mathbf{q}(\mathbf{a}^b, \mathbf{w}^b)\mathbf{q}^*, \tag{1}$$

where $\mathbf{a}$ and $\mathbf{w}$ denote the accelerations and gyroscopes, and b and g represent the body frame and Earth coordinate frame. In contrast, we retain the magnetometers in the body frame of IMU and apply a differential operation:

$$
\begin{aligned}
\dot{\mathbf{m}}^b &= \dot{\mathbf{R}} \cdot \mathbf{m}^g \\
&= \mathbf{\Omega} \cdot \mathbf{R} \cdot \mathbf{m}^g \\
&= \begin{pmatrix} 0 & -w_z & w_y \\ w_z & 0 & -w_x \\ -w_y & w_x & 0 \end{pmatrix} \cdot \mathbf{R} \cdot \mathbf{m}^g,
\end{aligned} \tag{2}
$$

where $\mathbf{\Omega}$ is the angular velocity matrix. Obviously, with the hidden rotation information, $\dot{\mathbf{m}}^b$ can be used to compensate for gyroscope drift as described in the aforementioned context.

Following with the combination of three-modality data as a time series, $\mathbf{X} = [\mathbf{a}^g; \mathbf{w}^g; \dot{\mathbf{m}}^b]$, which is then segmented into sequences of length L through a sliding window. The operation is done before the input, generating data samples

$\mathbf{X}_n \in \mathbb{R}^{L \times D}, n = [1, 2, 3, \cdots]$, where D is the IMU data dimension.

C. Model Architecture

We propose TF-BRT to improve the learning outcome for IMU-based robot tracking. TF-BRT comprises six key components, as shown in Fig. 3: time-frequency input projection, block-recurrent attention module, convolution module, multi-head attention module, feedforward module, and output projection layer. The time-frequency input projection extracts relevant information from both the time and frequency domains, capturing hidden features related to the robot's movement. The block-recurrent attention module incorporates RNN into the Transformer, allowing for pre-sequence extraction and contextual understanding of the current motion within the receptive field, which enables more accurate trajectory generation. To make the network convergence faster, the remaining four modules are interconnected in a residual way [23] with a pre-norm residual unit [24]. For the convolution module, a depthwise separable convolution [25] layer is sandwiched between the layernorm and dropout layer. Depthwise separable convolution can efficiently captures sequence's local features. The multi-head attention module employs a multi-head self-attention layer positioned between the layernorm and dropout layers. Finally, the feedforward module utilizes two fully-connected layers to extract the final features. After all the processes are completed, the output projection layer effectively distills the robot's velocity information from the high-dimensional space, resulting in the velocity sequence $\mathbf{V}_n$. This design approach excels in handling long-time sequences and shows promising generalization abilities in various environments.

1) Time-Frequency Input Projection: Recent studies on time series prediction and classification have emphasized the importance of incorporating frequency domain information. It has been suggested that the distinct patterns of various time series can be expressed through the frequency domain for an enhanced performance [26]–[28]. One such approach, UniTS [26], incorporates Short-Time Fourier Transform (STFT) in its convolution kernel coefficient initialization and demonstrates improved performance in IMU motion recognition when compared to models relying solely on time domain information.

Inspired by prior research, TF-BRT utilizes dual-channel inputs consisting of both time and frequency domain features. However, unlike UniTS and RF-Net [27], which use STFT and FFT as separate methods to extract frequency features, TF-BRT utilizes Discrete Cosine Transform (DCT) to extract frequency domain information. This choice avoids the need for complex number operations within neural networks.

The two input channels are connected by projection layers, which extract hidden features in the two channels through the fully connected layer and map the IMU feature domain ($\mathbb{R}^{L \times D}$) to a larger domain ($\mathbb{R}^{L \times D_h}$), enabling subsequent networks to effectively learn and operate within the expanded high-dimensional feature space. D_h represents the feature dimension in the following modules. The data after the projec-

tion layers are merged together to combine the extracted high-dimension features of the time domain and frequency domain. This operation can be written as $f_{\theta_t}(\mathbf{X}_n) + f_{\theta_f}(\text{DCT}(\mathbf{X}_n)) = \mathbf{M}_n$, where θ_t and θ_f denote the projection layer parameters of time channel and frequency channel, respectively, and $\mathbf{M}_n$ represents the merged hidden features.

2) Block-Recurrent Attention Module: Our model borrows the key framework of the block-recurrent transformer [22] to leverage the advantages of both RNN and self-attention mechanisms. Furthermore, we incorporate relative position encoding [29] as an additional component to augment the input features of the block-recurrent transformer. This encoding improves the representation of temporal order in the model. The block-recurrent attention module follows a pre-norm residual unit in a sandwich format. Specifically, the merged hidden features $\mathbf{M}_n$ from the merge layer are first normalized using a layernorm operation. The normalized hidden features, or the input embedding for the next layer, can be expressed as follows:

$$\mathbf{E}_n = \text{LayerNorm}(\mathbf{M}_n) \qquad (3)$$

Then the block-recurrent attention layer receives two inputs: the input embedding $\mathbf{E}_n \in \mathbb{R}^{L \times D_h}$ and the current state $\mathbf{S}_n \in \mathbb{R}^{L \times D_h}$. The input embedding captures the hidden information of the IMU data in the current window segmentation, while the current state embeds the hidden information of all previous sequences. To generate the output embedding $\mathbf{E}_{n+1}$ and the next state $\mathbf{S}_{n+1}$, two distinct steps are performed, which is shown in Fig. 4a and Fig. 4b. To obtain $\mathbf{E}_{n+1}$, the cross-attention result of the two inputs, and the multi-head self-attention [30] result of the input embedding are first concatenated, which can be expressed as:

$$\begin{aligned}\mathbf{H}_n = \text{Cat}(\text{CrossAttn}(\text{RPE}(\mathbf{E}_n), \text{RPE}(\mathbf{S}_n)), \\ \text{MultiAttn}(\text{RPE}(\mathbf{E}_n)))\end{aligned} \qquad (4)$$

where RPE denotes the relative position encoding [29], which maps an order of indexes to the input sequences. After passing through a projection layer, $\mathbf{H}_n$ is merged with $\mathbf{E}_n$, and the output embedding is finally obtained through a multilayer perceptron (MLP) layer based on residual format:

$$\mathbf{E}_{n+1} = \text{Res}(\text{MLP}(\text{Proj}(\mathbf{H}_n) + \mathbf{E}_n)) \qquad (5)$$

Fig. 4b gives the workflow for the next state $\mathbf{H}_{n+1}$. The only difference is that it utilizes LSTM gate. In addition, RNN structure allows the state tensor to selectively merge the current and previous information, providing essential information for future prediction. It should be noted that all of these tensors share the space of $\mathbb{R}^{L \times D_h}$. Finally, $\mathbf{E}_{n+1}$ is sent to the next module after the dropout layer.

D. Multi-Loss Learning

To improve TF-BRT's regression performance for estimating moving velocities and heading orientations, we employ a multi-loss learning strategy. The multi-loss function consists of three components: velocity loss $\mathcal{L}_v$, position loss or integrated velocity loss $\mathcal{L}_p$, and orientation loss $\mathcal{L}_o$.
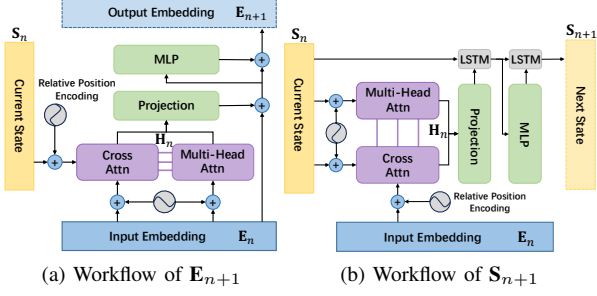
(a) Workflow of $\mathbf{E}_{n+1}$ (b) Workflow of $\mathbf{S}_{n+1}$

Figure 4: Block-Recurrent Attention Layer

Velocity Loss $(\mathcal{L}_v)$**:** With a predicted velocity sequence $\mathbf{V}_n = \{v_1, v_2, ..., v_L\}$, a mean square loss is utilized to measure the difference between the ground truth velocity $\mathbf{V}_n^g = \{v_1^g, v_2^g, ..., v_L^g\}$. The velocity loss function can be written as $\mathcal{L}_v = \sqrt{\frac{1}{L} \sum_{i=1}^{L} (v_i - v_i^g)^2}$.

Position Loss $(\mathcal{L}_p)$**:** The predicted velocity is integrated to obtain the predicted moving trajectory $\mathbf{P}_n$. By using $\mathcal{L}_p$, we aim to further reduce the cumulative error based on the learned velocity characteristics. The equation for $\mathcal{L}_p$ is $\mathcal{L}_p = \sqrt{\frac{1}{L} \sum_{i=1}^{L} (p_i - p_i^g)^2}$.

Orientation Loss $(\mathcal{L}_o)$**:** The major prediction errors come from direction deviations, especially at low speeds. For instance, even if the velocity loss is comparable to that at high speeds, the actual orientation error can be substantial due to the division of velocity error by the velocity modulus. To address this issue, we incorporate orientation loss to improve the accuracy of the predicted velocity in the travel direction. The definition of $\mathcal{L}_o$ is as follows: $\mathcal{L}o = \sqrt{\frac{1}{L} \sum i = 1^L (\frac{v_i}{||v_i||_2} - \frac{v_i^g}{||v_i^g||_2})^2}$.

The final multi-loss function is a linear combination of the above three loss functions. In order to better balance the different loss functions and optimize the final results, we utilize the variation coefficient [31] and define the multi-loss function as:

$$\mathcal{L}_{total} = \frac{\sigma_{\mathcal{L}_v}}{\mu_{\mathcal{L}_v}} \mathcal{L}_v + \frac{\sigma_{\mathcal{L}_p}}{\mu_{\mathcal{L}_p}} \mathcal{L}_p + \frac{\sigma_{\mathcal{L}_o}}{\mu_{\mathcal{L}_o}} \mathcal{L}_o \tag{6}$$

where μ and σ denote the mean and standard deviation of the respective loss function. The reason for applying both velocity loss and position loss is that $\mathcal{L}_v$ corrects the velocity vector on each frame, while $\mathcal{L}_p$ corrects it on a time window scale. By combining local and global information, the model can better learn the characteristics of the motion. A more detailed ablation analysis can be found in §VI-C later.

E. Data Augmentation

To improve the robustness of TF-BRT under different heading directions, both IMU data $\mathbf{X}_n$ and ground truth velocity $\mathbf{V}_n^g$ are randomly rotated by an angle of $\phi \in [0, 2\pi)$ on the floor plane [32]:

$$\Delta\mathbf{q}\mathbf{V}_n^g\Delta\mathbf{q}^* = \Delta\mathbf{q}\mathbf{X}_n\Delta\mathbf{q}^*, \tag{7}$$

where $\Delta\mathbf{q}$ represents the random rotation in quaternion. By taking this data augmentation method, the moving orientation will distribute more evenly on the floor plane, thus making the model more robust. We conduct an ablation study of the data augmentation method in §VI-D, which further verifies our consumption.

IV. IMPLEMENTATION

Data Collection: We build a customized robot platform for data collection, which captures raw IMU data as NEURIT input, visual-inertial tracking results from a commercialized device (Tango Phone[1]) for comparison, and the ground truth data from a LiDAR-inertial navigation system based on FAST-LIO [2]. We choose the Tango phone and FAST-LIO for specific reasons. The Tango phone has been used as a ground truth in inertial tracking datasets like RIDI and RONIN. FAST-LIO is known for its minimal drift in indoor environments.

Fig. 5a illustrates the system setup. The main component of the system is an Intel NUC with an i7-1260P CPU. By obtaining point clouds through LIVOX MID360 (FOV: 360°*59°)[2] and the built-in IMU, the FAST-LIO algorithm, which runs on the NUC, can accurately determine the indoor location of the robot. HiPNUC CH110 9-axis IMU is set on the left side, which records the raw data for model input. The Tango Phone set in the front is used to collect visual-inertial tracking results for comparison in §VI-F. In addition, we add AVIA (FOV: 70.4°*77.2°)[3] , a narrow-FOV LiDAR, to demonstrate the fact that LiDAR-inertial tracking systems cannot work well in simple and plain indoor environments. The robot's territory is AgileX Tracer-Mini, whose size is $40cm \times 40cm \times 26cm$ with a maximum speed of 1.5m/s.

Model Training: Models are implemented using PyTorch 1.7.1 and Cuda 11 in Python. The experiments are run using NVIDIA 4090 with 24GB GPU memory. We use the same training settings for all baselines, with a batch size of 72, an initial learning rate of 0.0003, and the ADAM optimizer while reducing the learning rate by a factor of 0.75 if the validation loss does not decrease in 10 epochs.

V. EXPERIMENTS

In the part of experimental analysis, the model proposed in this paper is analyzed comprehensively under different data sets and different indicators. Furthermore, it includes a comparison of the model with the visual positioning algorithm in complex indoor scenes, as well as an ablation study of the model itself. The study also involves the system setup and the evaluation of the real-time system.

A. Datasets

Due to the lack of IMU datasets on robots subject, we build our own dataset to verify the effectiveness of TF-BRT. We

---

[1]https://www.lenovo.com/il/en/tango/

[2]FOV: 360°*59°; Point Cloud Density: 40-line. https://www.livoxtech.com/mid-360

[3]FOV: 70.4°*77.2°; https://www.livoxtech.com/avia
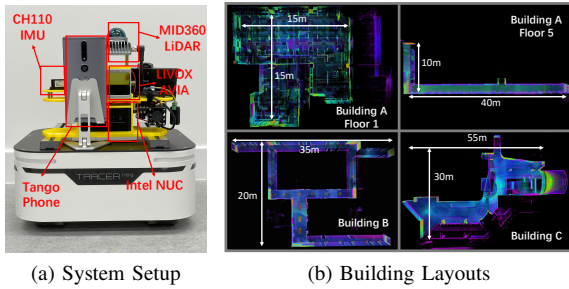
(a) System Setup   (b) Building Layouts

Figure 5: Experimental Settings. The floorplans are visualized based on the results reconstructed by FAST-LIO.
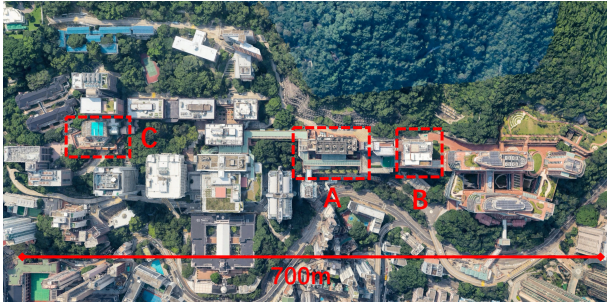

Figure 6: Topview of the locations of three buildings.

split the dataset into four parts, i.e. training, validation, test-seen and test-unseen set. More details are described below:

NEURIT: We build our own NEURIT dataset using the customized robotic platform in four floors across three buildings, which feature different layouts, environments, and floor conditions, as shown in Fig. 5b. The locations of these three buildings are illustrated in Fig. 6. We collect the training, validation, and test-seen sets in two floors of Building A, and build the test-unseen set in Building B and C. During data collection, the robot moves at varying speeds up to the maximum value (1.5m/s). The dataset contains 110 sequences, totaling around 15 hours of tracking data that corresponds to a travel distance of about 33.7 km. Each sequence of data lasts 6∼10 minutes. The ratio of the training set, validation set, test-seen set, and test-unseen set is 15:3:3:4.

RIDI: RIDI contains walking data of 10 human participants. We follow the default split setting in this dataset, which is 5:1:2:1.

RONIN: RONIN involves 100 human subjects. It is divided according to the default setting, *i.e.*, 69:16:35:32. It should be noted only 50% of the dataset has been released.

During the training stage, we divide the NEURIT and RIDI according to the segmentation size of 200×15 and the step size of 400, and slides 15 times according to the window size of 200 on each segment sequence. We partition RONIN dataset according to the partition size of 400×20 and the step size of 1000, and slide 20 times on each partition sequence according to the window size of 400. During the test stage, we use the same window size and step size of 200 for NEURIT and RIDI,

Table I: Summary of datasets

Dataset	Year	IMU Carrier	Sample Frequency	# of Sequences	Ground Truth
NeurIT	2023	CH110	200 Hz	110	FAST-LIO
RIDI	2017	Lenovo Phab2 Pro	200 Hz	98	Google Tango phone
RONIN	2019	Galaxy S9, Pixel 2 XL	200 Hz	118	Asus Zenfone AR

while a window size and step size of 400 for RONIN.

B. Baselines

To comprehensively evaluate NEURIT, we compare it with six state-of-the-art baseline approaches.

- **Naive Double Integration (NDI):** NDI [33] calculates current motion by integrating gyroscopes and accelerations.
- **Extended Kalman Filter (EKF):** EKF [7] filters out Gaussian-like noise in the IMU data and combines it with the magnetometer to correct the orientation error.
- **IONet:** IONet [10] employs RNN and fully-connected layers for model design. It only takes accelerations and gyroscopes as input features.
- **RONIN (Bi-LSTM):** We adopt the Bi-LSTM model that reports the best performance in RONIN [9] dataset. Only accelerations and gyroscopes are taken as input in RONIN.
- **UniTS:** UniTS [26] is an STFT-inspired neural network for sensory time series classification. UniTS takes accelerations and gyroscopes as inputs, the same as IONet and RONIN.
- **RF-Net:** RF-Net [27] is designed for wireless sensing, which learns from time-frequency representations. Only accelerations and gyroscopes are taken as input features.

It should be noted that Transformer-based solutions, such as CTIN [14] and A2DIO [15], even though they achieve promising results in inertial tracking, the model cannot be reproduced without implementation details and the source code. In this case, we do not include them as baseline models. We will evaluate the performance comparison with Transformer-based methodology in the ablation study §VI-C.

C. Evaluation Metrics

The evaluation mainly focuses on the predicted locations **P** derived from **V**. Particularly, we consider four common criteria to assess the error between the estimated positions **P** and the ground truths $\mathbf{P}^g$.

- **Absolute Trajectory Error (ATE)**: ATE [34] calculates the root mean square error (RMSE) of the predicted trajectory and the ground truth trajectory, which is given as $\sqrt{\frac{1}{n}\sum_i \|p_i - p_i^g\|_2^2}$.
- **Relative Trajectory Error (RTE)**: RTE [34] measures the RMSE between the predicted trajectory and the ground truth over a time-interval. RTE can be calculated as $\sqrt{\frac{1}{n}\sum_i \left\|(p_{i+\Delta t} - p_i) - (p_{i+\Delta t}^g - p_i^g)\right\|_2^2}$, where Δt is set to 60s in our evaluation.
- **Position Drift Error (PDE)**: PDE [14] computes the final position drift over the whole sequence. It can be expressed as $\|p_N - p_N^g\|_2 / D$, where N is the last index of the sequence, and D denotes the ground truth trajectory length.

- **Absolute Yaw Error (AYE)**: AYE [35] measures the RMSE between the heading orientations between ground truth and predicted trajectories, *i.e.*, $\sqrt{\frac{1}{n}\sum_i \left\| \frac{v_i}{\|v_i\|_2} - \frac{v_i^g}{\|v_i^g\|_2} \right\|_2^2}$.

VI. EVALUATION

A. Overall Performance

Evaluation on NEURIT Dataset: Tab. II shows the overall evaluation on NEURIT dataset. As seen, NEURIT produces remarkable accuracy on both seen and unseen test data, with a PDE of nearly 0.08, which implies an average error of only 0.8cm for every 1m traveled. NEURIT significantly reduces the average ATE by 62% over the best baseline approach. The extremely low values of RTE indicate a tiny drift of around 0.6% (0.6m drift over 1 minute of tracking). While UniTS (best baseline) can only achieve RTE results of approximately 1.5m, which is more than double. Furthermore, thanks to the multi-loss learning, NEURIT observes the improvement in AYE. NEURIT reduces the heading error by around 20%, from 43° (IONet) to 33°, indicating effective orientation error correction. Even without integrating magnetometers as input features, NEURIT outperforms the best baseline approach by an average of 30% across four metrics. For instance, by incorporating differential magnetometers, NEURIT achieves much greater performance enhancements, especially the results of RTE, which are almost reduced by 50%. These outcomes underscore the effectiveness of our sensor-fusion design.

To provide a more comprehensive visualization of the results, we include the cumulative distribution function of ATE and RTE in Fig. 7. The plots demonstrate that NEURIT surpasses all baseline models in terms of accuracy and reliability, particularly in unseen test sets. Even in the worst case, NEURIT outperforms the best-case performance of the other baseline models. We visualize some examples of the predicted trajectories in Fig. 8, to illustrate the stable tracking ability of NEURIT. The visualizations depict that the tracking trajectories generated by NEURIT closely match the ground truth trajectories. In contrast, other methodologies exhibit significant deviations, indicating their inability to track the robot's movement.

An additional comparison among the baseline models also demonstrates the shortcomings of using RNN or Transformers only, for inertial tracking. For instance, UniTS almost performs the best among all baseline models, however, it suffers from significant AYE and also fails in certain cases, resulting in long-tail drift errors. In contrast, by combining the advantages of RNN and Transformer, NEURIT can achieve state-of-the-art accuracy and robustness.

Evaluation on RIDI & RONIN Datasets: While we mainly focus on robotic tracking in this paper, we also test NEURIT on pedestrian tracking datasets to verify the effectiveness of our model design. Tab. III shows the test results on RIDI and RONIN datasets. NEURIT achieves the best performance among all baseline models. While the baselines also achieve reasonable accuracy for seen data, their performance degrades significantly for unseen data, for which NEURIT exceeds them

considerably. Specifically, in RIDI dataset, the performance gain increases from 17% on the seen test set to nearly 25% on the unseen test set. As for RONIN dataset, it's worth noting that the authors only made half of the total datasets available. Consequently, the model might not be able to fully capture the essential features of pedestrians, leading to a slight decrease in performance gains on the test unseen conditions. The noticeably inferior results on the RONIN dataset, compared to the results on the RIDI dataset, can be attributed to this fact as well. In conclusion, the obvious enhancement achieved by NEURIT demonstrates the potential of NEURIT to serve as a unified model for both robotic and pedestrian tracking.

B. Benchmark Study

Performance over Time and Distance: In this study, we examine the growth of prediction errors over time and tracking distance. As depicted in Fig. 9a and Fig. 9b, our prediction errors, like other tracking systems, increase with time and distance. Nonetheless, NEURIT experiences a much slower growth rate compared with the best baseline approach (UniTS). For example, the ATE of NEURIT after tracking for 250 meters is still smaller than that of the best baseline at 50 m. At a distance of 250 meters or after 5 minutes of travel, NEURIT keeps the mean trajectory error to around 0.9m. In contrast, the best baseline model achieves a similar error in just 1 minute and reaches an error of approximately 2.6m after 5 minutes (around 250m). The results indicate the stability and robustness of NEURIT over long-time or long-distance tracking in indoor environments.

Velocity Prediction Error: To assess NEURIT's performance in speed estimation, we calculate the ground truth for each moment and evaluate the error in the predicted speed. As shown in Fig. 10a, NEURIT yields a consistently higher speed accuracy than the best baseline (UniTS), with a considerable margin of around 0.2 m/s. The error in speed estimation remains constant until the actual speed exceeds 1.2 m/s while remaining within a narrow range of less than 0.4 m/s. Insights from the velocity probability density function indicate that the error grows at higher speeds, potentially due to insufficient training data in that range. Augmenting the dataset with more high-speed instances could be a potential solution to address this issue. Conversely, the best baseline performs poorly in speed estimation, with an average error of over 2 m/s across all speed conditions. In Fig. 10b, a brief analysis of a tracking trajectory shows that NEURIT generates a precise and accurate path that closely matches the ground truth. In contrast, the trajectory produced by the top baseline model exhibits erratic and imprecise movement.

Different Motion Status: The robot's movement status typically adapts to environmental changes. To evaluate the robustness of NEURIT in various indoor settings, we performed additional experiments and visualized the predicted trajectories along with the corresponding speed in Fig. 11. The office in Building A, floor 1 is narrow and crowded, the robot can only follow the narrow corridors. During turning and straight-line movement, NEURIT demonstrates excellent tracking ca-

Table II: Evaluation on NEURIT Dataset: (**Red**: the best performance among all algorithms. **Blue**: the best performance among all baseline models. Improvement is calculated based on the best baseline.)

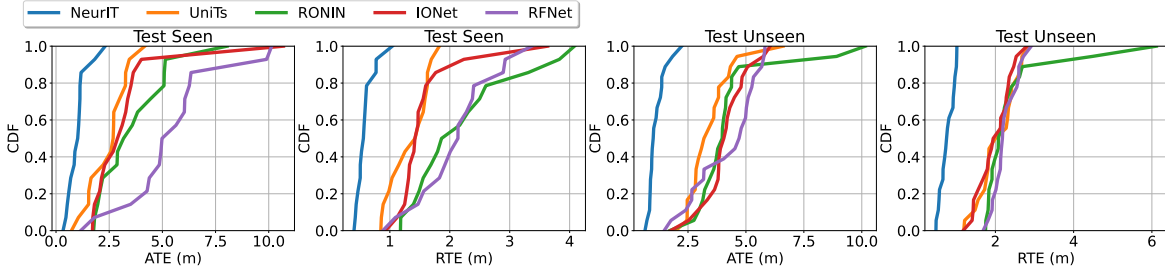| Dataset	Test Subject	Metric	NDI	EKF	RONIN	IONet	UniTS	RF-Net	NeurIT w/o magn	Impvt	NeurIT	Impvt
NeurIT Dataset	Seen	ATE	7.93	7.65	3.59	3.26	**2.71**	5.35	**1.53**	43.56% ↑	**1.01**	62.89% ↑
		RTE	10.01	9.61	2.19	1.58	**1.37**	2.09	**1.01**	26.18% ↑	**0.58**	57.31% ↑
		PDE	0.029	0.040	0.026	0.027	**0.021**	0.048	**0.010**	52.88% ↑	**0.007**	67.26% ↑
		AYE	123.09	124.77	63.77	**46.23**	121.41	99.76	**37.90**	18.02% ↑	**35.99**	22.15% ↑
	Unseen	ATE	9.24	8.96	4.26	3.45	**2.90**	4.12	**1.77**	39.11% ↑	**1.14**	60.89% ↑
		RTE	11.24	11.10	2.42	1.87	**1.74**	2.24	**1.61**	7.09% ↑	**0.76**	56.42% ↑
		PDE	**0.020**	0.036	0.035	0.027	0.023	0.035	**0.013**	36.81% ↑	**0.009**	55.70% ↑
		AYE	132.90	134.11	51.66	**40.10**	119.55	89.36	**33.58**	16.25% ↑	**32.14**	19.86% ↑

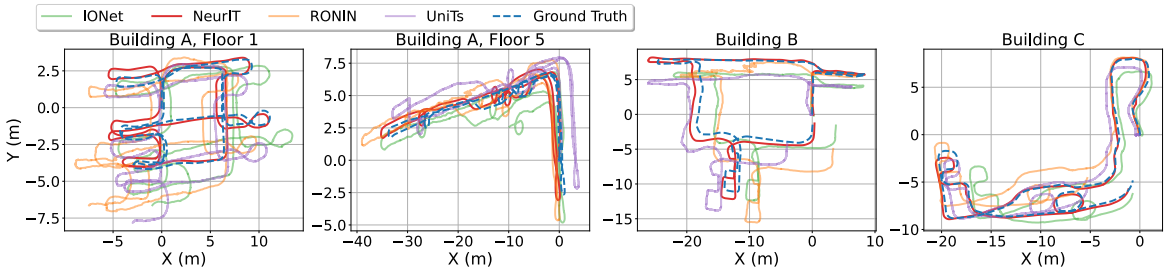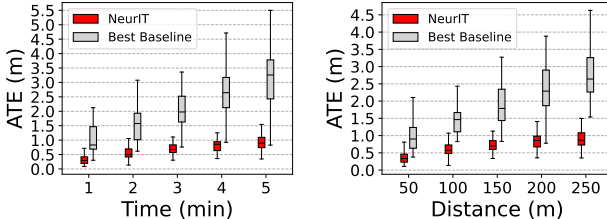Figure 7: CDF of ATE and RTE on NEURIT Test Dataset

Figure 8: Examples of Predicted Trajectories of NEURIT

(a) ATE of different moving time. (b) ATE of different moving distance.

Figure 9: Performance comparison between NEURIT and the best baseline model (UniTS) over time and distance.
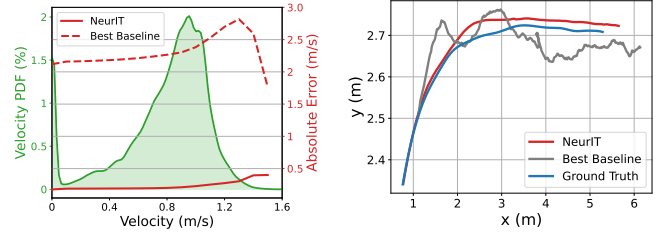

Figure 10: Velocity prediction comparison with the best baseline (UniTS). (a): Absolute velocity error at different speeds. (b): Comparison of predicted trajectories in 5s.

pabilities. It also exhibits reliable performance in challenging scenarios, including emergency starts, stops, and high-speed linear motion. Building A, floor 5 demonstrates an even more radical case with an extremely long and narrow corridor of approximately 40m. In the case of new environments, such as Building B and C, which represent complex and open areas, respectively, NEURIT is not affected by unseen conditions. These experiment outcomes showcase its robustness and adaptability in diverse indoor settings, even when confronted with previously unseen conditions.

C. Ablation Study

We proceed to evaluate the effectiveness of different design modules in NEURIT, focusing on four aspects: time-frequency input (TF), block-recurrent attention module (BR), multi-loss learning (m-loss), and a more detailed experiment on the impact of each loss function.

Time-frequency Input: To evaluate the effectiveness of time-frequency learning, we replaced the time-frequency dual channel with two time-domain channels. In doing so, we observed an increase in ATE from 1.08m to 1.49m, as shown in Fig.

Table III: Evaluation on RIDI & RONIN Datasets: (**Red**: the best performance among all algorithms. **Blue**: the best performance among all baseline models. Improvement is calculated based on the best baseline.)

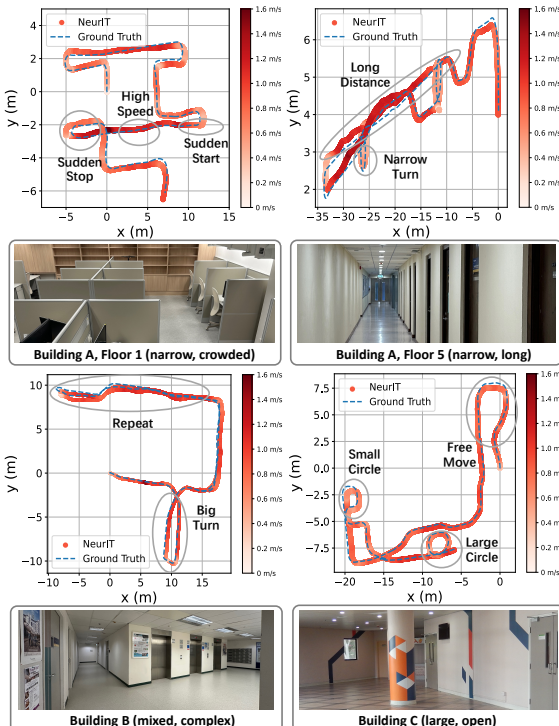| Dataset	Test Subject	Metric	NDI	EKF	RONIN	IONet	UniTS	RF-Net	NeurIT w/o magn	Impvt	NeurIT	Impvt
RIDI	Seen	ATE	16.75	26.04	1.72	1.76	1.66	3.94	1.63	1.40% ↑	1.53	7.64% ↑
		RTE	17.58	37.51	2.04	2.09	2.16	4.34	2.04	0.16% ↑	2.02	1.19% ↑
		PDE	0.2030	0.6836	0.0328	0.0319	0.0338	0.0688	0.0317	0.55% ↑	0.0286	10.41% ↑
		AYE	127.97	114.15	51.39	57.52	70.95	63.74	27.21	47.05% ↑	26.33	48.76% ↑
	Unseen	ATE	17.30	24.14	1.87	2.10	1.99	3.31	1.51	19.10% ↑	1.51	19.10% ↑
		RTE	18.02	40.67	1.87	2.18	1.92	3.20	1.66	11.16% ↑	1.60	14.50% ↑
		PDE	0.1799	0.7095	0.0291	0.0354	0.0310	0.0577	0.0278	4.62% ↑	0.0243	16.55% ↑
		AYE	130.59	105.93	48.47	53.67	67.42	64.64	24.34	49.78% ↑	24.21	50.05% ↑
RONIN	Seen	ATE	22.86	33.26	7.76	6.20	5.68	8.78	4.58	19.38% ↑	4.37	23.10% ↑
		RTE	30.49	35.10	3.19	3.17	2.77	6.43	2.60	6.03% ↑	2.59	6.53% ↑
		PDE	0.1240	0.1067	0.0432	0.0390	0.0267	0.0493	0.0216	18.99% ↑	0.0181	31.99% ↑
		AYE	122.48	120.96	63.12	74.49	107.92	86.91	46.56	26.24% ↑	47.60	24.59% ↑
	Unseen	ATE	17.30	33.47	8.91	7.73	6.38	10.27	5.78	9.52% ↑	5.35	16.26% ↑
		RTE	18.02	41.07	4.12	4.63	3.86	8.20	3.59	7.12% ↑	3.55	8.05% ↑
		PDE	0.0912	0.3166	0.0462	0.0358	0.0320	0.0592	0.0268	16.13% ↑	0.0243	24.03% ↑
		AYE	110.00	114.80	64.46	76.49	106.80	88.69	47.88	25.72% ↑	46.66	27.61% ↑

Figure 11: Visualization of robot motion status in different indoor environments.

13. The result confirms that representing sensory data in the time-frequency domain improves learning outcomes.

Block-recurrent Attention Module: We replace the Block-recurrent attention module with a self-attention module to evaluate its benefits. As shown in Fig. 13, this module contributes the most to the high performance of NEURIT. Compared to NEURIT, ATE, RTE of the ablation study decreased by 52.4%, and 94.7%, respectively. But even without Block-recurrent attention module, it still outperforms predictions without magnetometers. The results validate the advantages of combining RNN with Transformer in neural inertial tracking.
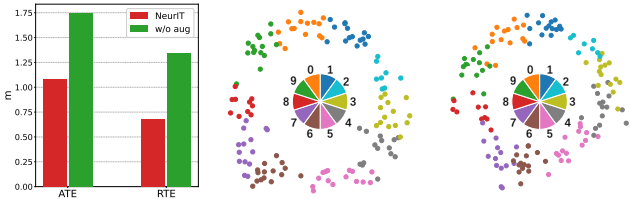
Multi-loss Learning: To evaluate the multi-loss learning, we first replace it with a single loss function, *i.e.*, position loss as used in RONIN. The performance degrades to a certain extent across the four evaluation metrics. We observe some counter-intuitive phenomena from the test results. Adding the loss function $\mathcal{L}_o$ to $\mathcal{L}_p$ resulted in a deterioration of the model's performance on ATE and RTE, despite an improvement in AYE from 35° to around 30°. This phenomenon is also observed with the loss combinations of $\mathcal{L}_o$ and $\mathcal{L}_v$ (without $\mathcal{L}_p$). One possible explanation for this observation is that including $\mathcal{L}_o$ in the loss function biases the model towards optimizing local orientation, which may affect the accurate estimation of global velocity. On the other hand, integrating $\mathcal{L}_p$ and $\mathcal{L}_v$ has a positive effect on improving the performance of NEURIT. Overall, the usage of these three loss functions strikes a balance between velocity vectors, trajectory errors, and heading orientations, allowing the model to predict the robot's trajectory most accurately.

D. Augmentation Study

In §III-E, we discussed the implementation of a data augmentation to improve the generalization ability on all orientations of the floor plane. In this section, we present comparative experiments on data augmentation to further validate our assumption. Fig. 12a illustrates the effect of data augmentation on ATE and RTE, which demonstrates that without data augmentation, the tracking error is approximately twice as large compared to when data augmentation is applied.

We perform extra experiments to explore how well neural networks can interpret IMU data across various heading directions. The 360-degree plane is divided into 10 groups, each covering a 36-degree range. The input data is classified into ten classes based on these groups. We focus on the output of the feedforward module, before the output projection layer. Then, we utilize t-SNE [36] to visualize the reduced dimensions of the extracted data in Fig. 12b and Fig. 12c. In Fig. 12c, the boundaries between groups appear blurred or mixed, particularly between Groups 3 and 4, which indicates that the model's ability to predict the robot's movement direction is imprecise without data augmentation. In contrast, Fig. 12b shows much clearer boundaries between different groups.

(a) Overall performance   (b) with augmentation   (c) without augmentation

Figure 12: Analyze the impact of the data augmentation. (a) shows the performance comparison on the test set with and without data augmentation. (b) and (c) are visualization results of hidden features, which are generated by Feedforward Block, using t-SNE. We take orientation as the features and separate it into 10 bins. The visualization results demonstrate that by using data augmentation, the model can have a better generalization capability of orientation on the floor plane.
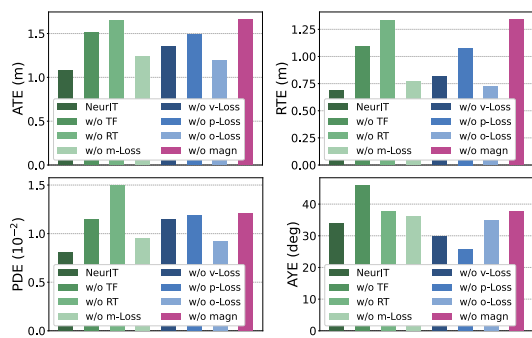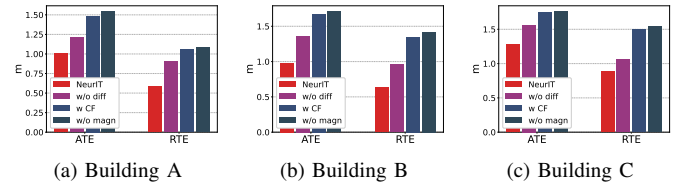

Figure 13: Ablation Study on NEURIT. The green bars: Modules in TF-BRT; Blue bars: Loss functions; Purple bar: Magnetometers.
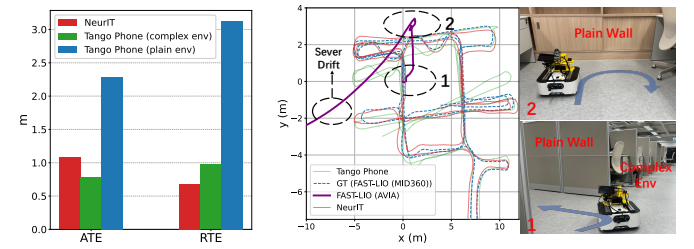
E. Magnetometer Study

In §II, we propose an orientation compensation method that differentiates the body-frame magnetometers as input features. It is mentioned that previous work [12], [16] used magnetometers for drift compensation as well, but in a complementary filter manner. To confirm the effectiveness of our method, we conducted two sets of comparative experiments. One uses the body-frame magnetometer as input without differentiation. The other employs a magnetometer-based complementary filter to correct the orientation error in the predicted trajectories. We experiment with three different buildings, with each trajectory lasting for more than 200m. The results are shown in Fig. 14. Obviously, our proposed method achieves optimal results in various scenarios. The results of **w/o diff** have a certain decrease (30%) compared to NEURIT but are still better than **CF** and **w/o magn**. Over long-distance tracking, the performance gains from the complementary filter are marginal, demonstrating its limitations in complex situations. The improvement is only 4% compared to not using magnetometers.

F. Comparison with Tango Phone and AVIA

We compared NEURIT with Tango phone's visual-inertial algorithm and the FAST-LIO algorithm using a narrow FOV

(a) Building A   (b) Building B   (c) Building C

Figure 14: Magnetometer study. **diff**: Differential operation; **CF**: Implementation of a complementary filter.

(a) Comparison on ATE, RTE   (b) Trajectory comparison

Figure 15: Comparison with Tango Phone and narrow-FOV LiDAR (AVIA).

LiDAR (AVIA). In an environment with many feature points, NEURIT performs similarly to Tango phone, achieving an ATE of 1.08m compared to Tango phone's 0.78m. However, in environments with limited visual feature points, NEURIT outperforms Tango phone. We did not report the results of AVIA-based FAST-LIO due to significant drift of hundreds of meters. Fig. 15b shows the estimated trajectories using various methods. Tango phone exhibits drift in corners with no visual points, while NEURIT remains consistent with the ground truth. The AVIA-based FAST-LIO algorithm is highly affected, with significant errors and severe drift after the second turn's plain wall, making trajectory tracking impossible for the robot.
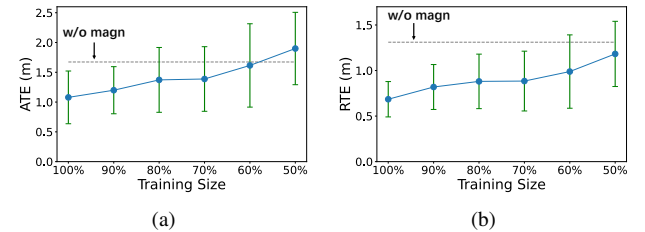

(a)   (b)

Figure 16: Analyze the impact of training size on overall performance. The gray dot line indicates the test results without taking magnetometers as input features.

G. Training Datasize

We also conduct experiments on the influence of the size of the training set on the model performance, and the experimental results are shown in Fig. 16. As the size of the training set decreased from 100% to 50%, the accuracy of the model to the tracking of the robot gradually decreased, in which ATE increased from 1.08m to 1.89m, and RTE increased from 0.68m to 1.18m. The gray dashed line indicates the test results

without taking magnetometers as input features. The findings reveal that when employing the magnetometers, approximately 60% of the training set attains comparable model performance as the case where the magnetometer is not implemented. Notably, even with a mere 50% of the training set, the model exhibits superior results in the realm of RTE when compared to the outcomes obtained without utilizing a magnetometer. These outcomes indicate the stability and remarkable generalization capability of our proposed methodology.

H. System Latency

Table IV: Power consumption and system complexity. The average time indicates the time consumption for predicting 1-second IMU data.

Indicator	Standby Mode	GPU Mode	CPU Mode
Total Power (W)	3.9	7.1	4.7
GPU & CPU Power (W)	0.56	2.4	1.3
Avg. time (ms)	\	34.48	783.4
CPU Usage (%)	\	\	118.71
Memory Usage (Mb)	\	\	372

To examine NEURIT as a real-time, power-efficient solution, we evaluate its end-to-end system complexity and power consumption on NVIDIA Jetson Orin Nano, which has been widely applied in robotic applications [37], [38], in a multi-ROS system with Intel NUC. As shown in Tab. IV, NEURIT requires 34.48ms to predict 1-second IMU data in GPU mode, including 1.62ms dedicated to coordinate system transformation and noise reduction. The results promise NEURIT as a real-time, power-efficient system to run on robotic things.

VII. RELATED WORKS

Inertial tracking has been proposed for many years. The Kalman filter [39], introduced in 1960, improved vehicle guidance and navigation control, including spacecraft orbit control in the Apollo program. Additional advancements, such as the extended Kalman filter [7], facilitated accurate navigation in nonlinear systems. However, when applied to low-cost IMUs on mobile phones, these algorithms perform poorly due to noise and complex pedestrian movements. To enhance phone attitude estimation, A^3 [40] utilized accelerations and magnetometers to calibrate gyroscope drift. Subsequent work, like MUSE [16], achieved promising results in device orientation tracking. These applications primarily focus on device orientation in specific areas, requiring careful calibration or parameter selection for optimal performance.

To realize indoor inertial tracking, machine learning and data-driven techniques have been exploited. RIDI [20], IONet [10], RONIN [9], and MotionTransformer [41] are examples of methods that employ deep learning and neural networks to estimate pedestrian motion trajectories. These methods have limitations in terms of generalization and applicability to other moving targets. Some studies [42] have combined neural networks with Kalman filters to improve prediction accuracy by learning noise parameters. However, the performance of existing methods still has room for optimization, particularly in handling unseen data and environments.

NEURIT takes a further step in this direction and pushes the limit of the state-of-the-art accuracy.

VIII. CONCLUSIONS

In this paper, we present NEURIT, a neural inertial tracking system that takes full advantage of IMU readings. We propose a novel Time-Frequency Block-recurrent Transformer, named TF-BRT, which borrows the idea of time-frequency learning and embraces the advantages of both RNN and Transformer to combine both historical and current motion information. In addition, we leverage the differentiation of the body-frame magnetometers to mitigate the noise introduced by the gyroscope. We implement NEURIT with a customized robotic platform and evaluate it scrupulously across distinct indoor environments. The results show that NEURIT outperforms six state-of-the-art baseline approaches on all benchmarks, achieving a significant accuracy gain of 48% on unseen data compared to the best baseline so far. NEURIT demonstrates remarkable tracking accuracy over extended durations and distances, with a tracking error of one meter over 300 meters, ensuring reliable performance. With the encouraging results, NEURIT takes an important step towards a practical and truly infrastructure-free solution for indoor robotic tracking.

REFERENCES

[1] C. Zhao, G. G. Yen, Q. Sun, C. Zhang, and Y. Tang, "Masked gan for unsupervised depth and pose prediction with scale consistency," *IEEE Transactions on Neural Networks and Learning Systems*, vol. 32, no. 12, pp. 5392–5403, 2020.

[2] W. Xu and F. Zhang, "Fast-lio: A fast, robust lidar-inertial odometry package by tightly-coupled iterated kalman filter," *IEEE Robotics and Automation Letters*, vol. 6, no. 2, pp. 3317–3324, 2021.

[3] C. Wu, F. Zhang, Y. Fan, and K. R. Liu, "Rf-based inertial measurement," in *Proceedings of the ACM Special Interest Group on Data Communication*, 2019, pp. 117–129.

[4] M. E. Rasekh, Z. Marzi, Y. Zhu, U. Madhow, and H. Zheng, "Noncoherent mmwave path tracking," in *Proceedings of the 18th International Workshop on Mobile Computing Systems and Applications*, 2017, pp. 13–18.

[5] H. Wymeersch, S. Maranò, W. M. Gifford, and M. Z. Win, "A machine learning approach to ranging error mitigation for uwb localization," *IEEE transactions on communications*, vol. 60, no. 6, pp. 1719–1728, 2012.

[6] N. Ahmad, R. A. R. Ghazilla, N. M. Khairi, and V. Kasi, "Reviews on various inertial measurement unit (imu) sensor applications," *International Journal of Signal Processing Systems*, vol. 1, no. 2, pp. 256–262, 2013.

[7] M. I. Ribeiro, "Kalman and extended kalman filters: Concept, derivation and properties," *Institute for Systems and Robotics*, vol. 43, no. 46, pp. 3736–3741, 2004.

[8] M. Euston, P. Coote, R. Mahony, J. Kim, and T. Hamel, "A complementary filter for attitude estimation of a fixed-wing uav," in *2008 IEEE/RSJ international conference on intelligent robots and systems*. IEEE, 2008, pp. 340–345.

[9] H. Yan, S. Herath, and Y. Furukawa, "Ronin: Robust neural inertial navigation in the wild: Benchmark, evaluations, and new methods," *arXiv preprint arXiv:1905.12853*, 2019.

[10] C. Chen, X. Lu, A. Markham, and N. Trigoni, "Ionet: Learning to cure the curse of drift in inertial odometry," in *Proceedings of the AAAI Conference on Artificial Intelligence*, vol. 32, no. 1, 2018.

[11] X. Wei and V. Radu, "Calibrating recurrent neural networks on smartphone inertial sensors for location tracking," in *2019 International Conference on Indoor Positioning and Indoor Navigation (IPIN)*. IEEE, 2019, pp. 1–8.

[12] J. Gong, X. Zhang, Y. Huang, J. Ren, and Y. Zhang, "Robust inertial motion tracking through deep sensor fusion across smart earbuds and smartphone," *Proceedings of the ACM on Interactive, Mobile, Wearable and Ubiquitous Technologies*, vol. 5, no. 2, pp. 1–26, 2021.

[13] J. Gonzalez and W. Yu, "Non-linear system modeling using lstm neural networks," *IFAC-PapersOnLine*, vol. 51, no. 13, pp. 485–489, 2018.

[14] B. Rao, E. Kazemi, Y. Ding, D. M. Shila, F. M. Tucker, and L. Wang, "Ctin: Robust contextual transformer network for inertial navigation," in *Proceedings of the AAAI Conference on Artificial Intelligence*, vol. 36, no. 5, 2022, 5413–5421.

[15] Y. Wang, H. Cheng, and M. Q.-H. Meng, "A2dio: Attention-driven deep inertial odometry for pedestrian localization based on 6d imu," in *2022 International Conference on Robotics and Automation (ICRA)*. IEEE, 2022, pp. 819–825.

[16] S. Shen, M. Gowda, and R. Roy Choudhury, "Closing the gaps in inertial motion tracking," in *Proceedings of the 24th Annual International Conference on Mobile Computing and Networking*, 2018, pp. 429–444.

[17] J. Chung, M. Donahoe, C. Schmandt, I.-J. Kim, P. Razavai, and M. Wiseman, "Indoor location sensing using geo-magnetism," in *Proceedings of the 9th international conference on Mobile systems, applications, and services*, 2011, pp. 141–154.

[18] X. Fan, J. Wu, C. Long, and Y. Zhu, "Accurate and low-cost mobile indoor localization with 2-d magnetic fingerprints," in *Proceedings of the First ACM Workshop on Mobile Crowdsensing Systems and Applications*, 2017, pp. 13–18.

[19] P.-F. Ho, C.-C. Wang, and J.-C. Chen, "Using magnetic fingerprints to position cars on multi-layer roads," in *Proceedings of the 26th Annual International Conference on Mobile Computing and Networking*, 2020, pp. 1–3.

[20] H. Yan, Q. Shan, and Y. Furukawa, "Ridi: Robust imu double integration," in *Proceedings of the European Conference on Computer Vision (ECCV)*, 2018, pp. 621–636.

[21] K. A. Nguyen and Z. Luo, "On assessing the positioning accuracy of google tango in challenging indoor environments," in *2017 international conference on indoor positioning and indoor navigation (IPIN)*. IEEE, 2017, pp. 1–8.

[22] D. Hutchins, I. Schlag, Y. Wu, E. Dyer, and B. Neyshabur, "Block-recurrent transformers," *arXiv preprint arXiv:2203.07852*, 2022.

[23] A. Gulati, J. Qin, C.-C. Chiu, N. Parmar, Y. Zhang, J. Yu, W. Han, S. Wang, Z. Zhang, Y. Wu *et al.*, "Conformer: Convolution-augmented transformer for speech recognition," *arXiv preprint arXiv:2005.08100*, 2020.

[24] Z. Dai, Z. Yang, Y. Yang, J. G. Carbonell, Q. V. Le, and R. Salakhutdinov, "Transformer-xl: Attentive language models beyond a fixed-length context," *ArXiv*, vol. abs/1901.02860, 2019.

[25] F. Chollet, "Xception: Deep learning with depthwise separable convolutions," in *Proceedings of the IEEE conference on computer vision and pattern recognition*, 2017, pp. 1251–1258.

[26] S. Li, R. R. Chowdhury, J. Shang, R. K. Gupta, and D. Hong, "Units: Short-time fourier inspired neural networks for sensory time series classification," in *Proceedings of the 19th ACM Conference on Embedded Networked Sensor Systems*, 2021, pp. 234–247.

[27] S. Ding, Z. Chen, T. Zheng, and J. Luo, "Rf-net: A unified meta-learning framework for rf-enabled one-shot human activity recognition," in *Proceedings of the 18th Conference on Embedded Networked Sensor Systems*, 2020, pp. 517–530.

[28] S. Yao, A. Piao, W. Jiang, Y. Zhao, H. Shao, S. Liu, D. Liu, J. Li, T. Wang, S. Hu *et al.*, "Stfnets: Learning sensing signals from the time-frequency perspective with short-time fourier neural networks," in *The World Wide Web Conference*, 2019, pp. 2192–2202.

[29] K. Wu, H. Peng, M. Chen, J. Fu, and H. Chao, "Rethinking and improving relative position encoding for vision transformer," in *Proceedings of the IEEE/CVF International Conference on Computer Vision*, 2021, pp. 10 033–10 041.

[30] A. Vaswani, N. Shazeer, N. Parmar, J. Uszkoreit, L. Jones, A. N. Gomez, Ł. Kaiser, and I. Polosukhin, "Attention is all you need," *Advances in neural information processing systems*, vol. 30, 2017.

[31] R. Groenendijk, S. Karaoglu, T. Gevers, and T. Mensink, "Multi-loss weighting with coefficient of variations," in *Proceedings of the IEEE/CVF winter conference on applications of computer vision*, 2021, pp. 1469–1478.

[32] X. Cao, C. Zhou, D. Zeng, and Y. Wang, "Rio: Rotation-equivariance supervised learning of robust inertial odometry," in *Proceedings of the IEEE/CVF Conference on Computer Vision and Pattern Recognition*, 2022, pp. 6614–6623.

[33] P. G. Savage, "Strapdown inertial navigation integration algorithm design part 2: Velocity and position algorithms," *Journal of Guidance, Control, and dynamics*, vol. 21, no. 2, pp. 208–221, 1998.

[34] J. Sturm, N. Engelhard, F. Endres, W. Burgard, and D. Cremers, "A benchmark for the evaluation of rgb-d slam systems," in *2012 IEEE/RSJ international conference on intelligent robots and systems*. IEEE, 2012, pp. 573–580.

[35] Y. Wang, J. Kuang, X. Niu, and J. Liu, "Llio: Lightweight learned inertial odometer," *IEEE Internet of Things Journal*, 2022.

[36] L. Van der Maaten and G. Hinton, "Visualizing data using t-sne." *Journal of machine learning research*, vol. 9, no. 11, 2008.

[37] G. Alexey, V. Klyachin, K. Eldar, and A. Driaba, "Autonomous mobile robot with ai based on jetson nano," in *Proceedings of the Future Technologies Conference (FTC) 2020, Volume 1*. Springer, 2021, pp. 190–204.

[38] J. Tang, Y. Ren, and S. Liu, "Real-time robot localization, vision, and speech recognition on nvidia jetson tx1," *arXiv preprint arXiv:1705.10945*, 2017.

[39] R. L. Stratonovich, "Optimum nonlinear systems which bring about a separation of a signal with constant parameters from noise," *Radiofizika*, vol. 2, no. 6, pp. 892–901, 1959.

[40] P. Zhou, M. Li, and G. Shen, "Use it free: Instantly knowing your phone attitude," in *Proceedings of the 20th annual international conference on Mobile computing and networking*, 2014, pp. 605–616.

[41] C. Chen, Y. Miao, C. X. Lu, L. Xie, P. Blunsom, A. Markham, and N. Trigoni, "Motiontransformer: Transferring neural inertial tracking between domains," in *Proceedings of the AAAI conference on artificial intelligence*, vol. 33, no. 01, 2019, pp. 8009–8016.

[42] M. Brossard, A. Barrau, and S. Bonnabel, "Ai-imu dead-reckoning," *IEEE Transactions on Intelligent Vehicles*, vol. 5, no. 4, pp. 585–595, 2020.